16th World Conference on Earthquake, 16WCEE 2017

Santiago Chile, January 9th to 13th 2017

Paper N° 509

Registration Code: S-S1461084063

SEISMIC FRAGILITY ANALYSIS FOR UNANCHORED TANKS CONSIDERING SHELL BUCKLING

G. Cortés[(1)], G.S. Prinz[(2)]

[(1)] *Assistant Professor, LeTourneau University, gcortes.dde@gmail.com*
[(2)] *Assistant Professor, University of Arkansas, prinz@uark.edu*

Abstract

When unanchored steel liquid storage tanks are subjected to strong ground motions, the contained liquid impulses the tank shell causing uplift of the tank base. As the tank undergoes uplift, sections of the shell that remain in contact with the ground can experience large compressive forces often leading to buckling failure. This phenomenon has been documented in several reconnaissance reports following major earthquakes. In these reports, two types of shell buckling are commonly encountered: 1) elastic buckling (sometimes referred to as diamond bucking from the distinct diamond pattern that often emerges in the tank shell), and 2) plastic buckling (also called elephant foot buckling from the deformed tank shape which resembles an elephants foot bulging out at the bottom).

This paper presents a method for determining the buckling vulnerability of unanchored steel tanks using simplified mass-spring models incorporated into the Open System for Earthquake Engineering Simulation (OpenSEES), and incremental dynamic analysis. The simplified mass-spring models simulate resistance to uplift, tank rocking, and provide an equilibrium-based approach to determining tank shell compressive forces resulting from dynamic earthquake loadings. Four existing tanks (considering both broad and slender geometries) are analyzed under 20 recorded ground motions, scaled at 30 different levels (from 0.05g to 1.5g) for a total of 2,400 dynamic analyses. Results from the incremental dynamic analyses are used to create fragility curves, wherein shell buckling probabilities are related to the level of seismic excitation. Results from the analyses on the four existing tank geometries highlight vulnerabilities for both broad and slender tank geometries under moderate seismic excitation.

Keywords: unanchored steel tanks; fragility curves; dynamic analysis; shell buckling

1. Introduction

When the liquid stored in large unanchored steel tanks is subjected to strong ground motion it reacts mainly by sloshing in an upper 'convective' layer and as an impulsive mass moving with the tank wall/shell [1, 2]. The sloshing motion of the upper liquid may cause damage to the roof and upper shell, while the impulsive liquid may cause damage to the lower shell and tank base.

This paper presents a simplified mass-spring model for determining seismic demands within the shell of an unanchored tank. The demands calculated from this model are then compared with the shell buckling capacity and fragility curves for probabilistic damage estimation are created.

The nonlinear mass-spring model used to analyze tank response to seismic loading is presented first. Next, a summary of the compressive capacity of the tank shell is presented. The fragility study on existing tank configurations having varied height-to-radius ratios (H/R ratios) and the ground motions used for analysis are then presented. The paper finishes with a discussion of the main results and conclusions.

2. Mass-Spring Model for Determining Compression Demand

Fig. 1 shows the mass-spring model, with the various components chosen to represent the dynamic response of the steel tank and liquid contents. The impulsive liquid mass is lumped to the end of an elastic beam element which represents the tank shell. The height of the lumped impulsive mass is calculated as described in [3]. Flexural stiffness for the elastic beam element representing the tank shell is chosen to match the tank natural frequency as determined from [4]. The elastic beam element is attached to a rigid link, as results from tilt tests on scaled tanks indicate that the shell of the tank rotates as a rigid body due to its large in-plane stiffness [5].

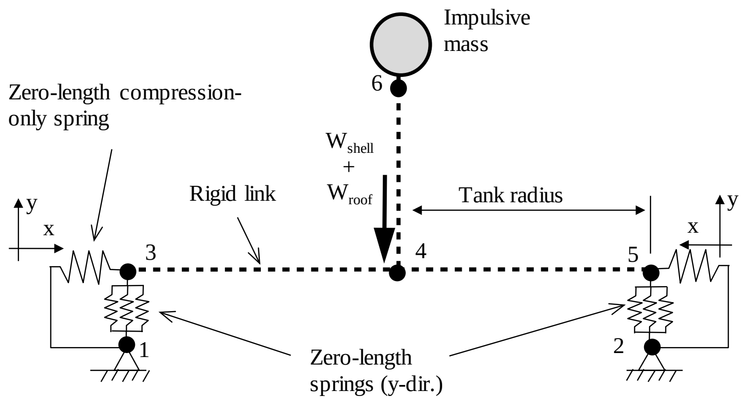

Fig. 1 – Rocking mass-spring model for simulating dynamic tank behavior.

A series of springs are added at each end of the base to provide uplift resistance and transfer the base accelerations to the impulsive mass (Fig. 1). The horizontal springs in the model (x-direction in Fig. 1) consist of compression only springs used to transfer the ground motion acceleration to the model. The vertical springs consider ground contact and resistance to uplift. When the full base of the tank is in contact with the ground (i.e., no uplift), uplift resistance is provided by the weight of the roof and the shell. While the tank undergoes uplift, resistance to overturning is provided by the weight of the liquid in the uplifted crescent of liquid (Fig. 2), along with the weight of the shell and the weight of the roof. The tank's moment resistance, before (M_0) and after uplift (M_{uplift}), is given by Eq. (1) and Eq. (2) respectively.

$$M_0 = (W_{shell} + W_{roof})R \tag{1}$$

$$M_{uplift} = W_s kR - W_f(R - r) \tag{2}$$

In Eq. (1) and Eq. (2), W_{shell} and W_{roof} are the weight of the tank shell and roof respectively, R is the tank radius, W_s is the total weight of the tank shell, roof and liquid over of the uplifted crescent (see Fig. 2), kR is the distance from the location of W_s to the center of the tank, W_f is the weight of the liquid in contact with the ground (not uplifted) and r is the radius of the base which is still in contact with the ground.

The shell compressive demand (f_{MAX}), given by Eq. (3) [3], is a function of the half angle, θ^*, which is inversely proportional to tank uplift. θ^* defines the arc of the shell base in contact with the foundation and is obtained from equilibrium between the overturning moment, given by the mass-spring model, and the restoring moment from the steel self-weight, uplifted liquid, and non-uplifted liquid, as shown in Fig. 2.

$$f_{MAX} = \left(\frac{C \cdot W_S}{R \cdot \theta^* t_s} \right) \cdot CF \tag{3}$$

In Eq. (3), C is a foundation stiffness factor (assumed 1.0 for the rigid foundations found in the tanks studied), t_s is the shell thickness, and *CF* is an empirical constant taken as 2.5 for all analyses in this study, as suggested by [6].

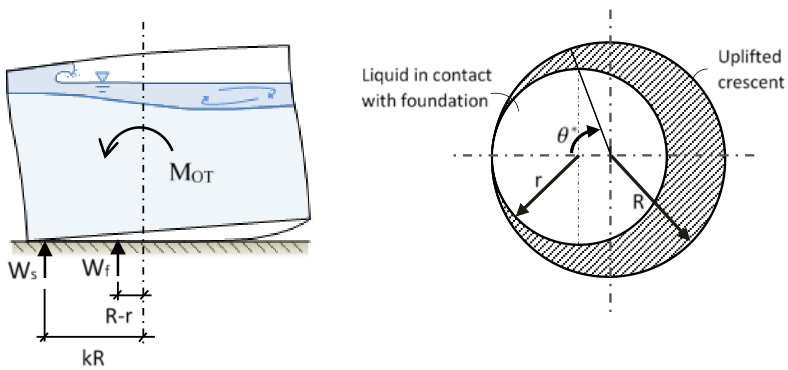

Fig. 2 – Resultant forces under rocking motion.

3. Shell Buckling Capacity

The limit states of compression yielding, elastic and elastic-plastic shell buckling were considered. Elastic buckling, sometimes referred to as diamond bucking because of the distinct diamond pattern that emerges in the tank shell, is determined by means of Eq. (4), described by [7] and specified in [3, 4].

$$f_m = \left(0.19 + 0.81 \frac{f_p}{f_{c1}}\right) f_{c1} \tag{4}$$

Where f_{c1} is the ideal critical buckling stress for cylinders loaded in axial compression and f_p expresses the increase in buckling stress due to internal hydraulic pressure.

Elastic-plastic buckling is caused by a combination of compression stresses, tensile hoop stresses and high shear at a location near the base of the tank. This buckling mode is often called elephant foot buckling since the buckled tank shape resembles an elephant's foot bulging out at the bottom. The elastic-plastic capacity is given by Eq. (5):

$$f_m = f_{c1} \left[1 - \left(1 - \frac{pR}{t_s f_y}\right)^2\right] \left(1 - \frac{1}{1.12 + r^{1.15}}\right) \left[\frac{r + f_y/250}{r+1}\right] \tag{5}$$

Where:

$$r = \frac{R/t_s}{400} \quad (6)$$

R is the tank radius, p is the fluid pressure at the tank base, t_s is the shell thickness and f_y is the yield strength of the shell (expressed in MPa).

In addition to elastic and elastic-plastic buckling of the shell, compression yielding of the shell was also verified but did not control for any of the tanks studied.

4. Fragility Analysis

Fragility curves were used to relate the level of seismic intensity to the probability of structural damage (i.e. shell buckling). The peak ground acceleration (PGA) was chosen as the intensity measure, and earthquake ground motions scaled to multiple PGA levels were used to generate demands in the tank mass-spring model. Damage limit states considered in the study include elastic and elastic-plastic buckling of the shell as discussed in the previous section. The probability of damage was calculated for the limit states at each discrete level of intensity (PGA). A lognormal cumulative distribution, given by Eq. (7), was used to represent the damage probability as described in [8].

$$P(D|PGA) = \Phi\left(\frac{ln(PGA/\mu)}{\sigma}\right) \quad (7)$$

In Eq. (7), P(D/PGA) is the probability that a ground motion of a given PGA value will cause structural damage (i.e., shell buckling), Φ is the standard normal cumulative distribution function, μ is the median of the fragility function and σ is the standard deviation of the corresponding lognormal distribution.

5. Tank Geometries

The seismic vulnerability of existing unanchored tanks was investigated using the analysis approach explained in previous sections. Four tanks with different geometries, shown in Table 1, were chosen from seismic prone regions throughout Switzerland, representing both slender and broad tank geometries. Table 1 shows the four tanks, along with the year of construction, the main dimensions, the shell thicknesses relevant to the shell buckling analysis, and the shell yield strength.

Table 1 – Geometry and material properties of existing tanks for fragility study

Tank ID	Construction Year	Height, H [m]	Radius, R [m]	H/R	Volume, V [m^3]	t_{lc} [a] [mm]	t_{eq} [b] [mm]	t_b [c] [mm]	f_y [MPa]
St-Triphon	1951	16.2	14.5	1.12	10,700	24	17.7	10	235
Rumlang	1975	26.3	15.0	1.75	18,600	16	11.8	12	355
Birsfelden	1955	19.4	9.0	2.16	5,000	16	11.9	10	235
Vernier	1995	20.0	5.75	3.48	2,080	7	6.9	7	235

a. Tank shell thickness in the lower course
b. Equivalent tank shell thickness taken as average of lower and upper shell courses
c. Tank base-plate thickness

6. Ground Motions

Twenty recorded earthquake ground motions were chosen for the tank fragility analysis. All ground motions consider combinations of magnitude and distance based on the site de-aggregation of Sion, Switzerland. The chosen de-aggregation considers a return period of 2,500 years (2% probability of exceedance in 50 years) and soil class types C and D, which have an average shear wave velocity below 500m/s in the soil's upper 30m [9]. Selected ground motions were chosen from shallow earthquakes with focal depths less than 20 km. Table 2 presents the twenty ground motions along with relevant information about the station, magnitude, distance, depth, and soil type.

To generate fragility curves based on earthquake intensity, each of the twenty ground motions were normalized by peak ground acceleration (PGA) and then scaled to have PGAs varying from 0.05g to 1.5g. This resulted in 30 different intensities for each of the 20 ground motions and a total of 600 dynamic analyses for each tank.

Table 2 – Ground motions for nonlinear dynamic analysis

Event Name	Station	NGA # [a]	Date	M_W [b]	Distance (km)	Depth (km)	Vs,30 [c] (m/s)
13.05.1997	Sendai	-	13.05.97	6.2	15	8	D
25.06.1997	Ikumonaka	-	25.06.97	6.1	10	12	D
26.07.2003	Tsuwano	-	26.07.03	6.1	10	12	C-D
26.07.2003	Ishinomaki	-	26.07.03	6.2	10	12	C-D
23.10.2004	Ojiya	-	23.10.04	6.5	12	14	C
26.03.1997	Miyanojoh	-	26.03.97	6.3	12	8	C
23.10.2004	Kawanishi	-	23.10.04	6	12	12	C
L'Aquila	AM043	-	04.06.09	6.3	7.9	8.8	-
Friuly, Italy - 01	Tolmezzo	125	05.06.76	6.5	15.8	20.9	424.8
Friuli, Italy - 02	Buia	130	09.15.76	5.9	11	0.9	338.6
Friuli, Italy - 02	Forgario Cornino	132	09.15.76	5.9	14.8	0.9	412.4
Norcia, Italy	Spoleto	157	09.19.79	5.9	13.4	15	338.6
Irpinia, Italy - 01	Brienza	288	11.23.80	6.9	22.6	6.9	500
Irpinia, Italy - 02	Calitry	300	11.23.80	6.2	8.8	6.9	600
Irpinia, Italy - 02	Rionero In Vulture	302	11.23.80	6.2	22.7	6.9	530
Coyote Lake	Gilroy Array #2	147	08.06.79	5.7	9.0	7.5	271
Coyote Lake	Gilroy Array #3	148	08.06.79	5.7	7.4	7.5	350
Westmorland	Salton Sea Wildlife Refuge	317	04.26.81	5.9	7.8	10.1	191.1
Coalinga-05	Oil City	407	07.22.83	5.7	8.5	7.3	376.1
San Salvador	National Geografical Inst	569	10.10.86	5.8	7.0	10.9	350

[a.] "Next generation attenuation" number
[b.] Earthquake moment magnitude
[c.] Average shear-wave velocity between 0 and 30m of depth

7. Results

Dynamic analyses of the four tanks subjected to the 20 ground motions identified in Table 2, scaled to have PGAs varying from 0.05g to 1.5g, were performed. For each analysis the maximum compression demand at the tank shell was determined and compared against the capacity given by Eqs. (4) and (5). The percentage of the 20 ground motions that caused compressive shell failure (for each tank) was calculated at every PGA intensity, as shown by the discrete data points in Fig. 3. Fragility curves were determined by means of Eq. (7) for each tank and are also shown in Fig. 3. The median and the standard deviation (μ, σ) were determined by minimizing the sum of the differences between the discrete data points and the fragility curve using the Generalized Reduced Gradient nonlinear optimization code.

Fragility curves provide the probability of reaching shell compressive failure for a ground motion of given PGA. As could be expected, the most slender tank has the highest probability of shell compressive failure while the least slender tank has the least probability of failure. While slenderness is an important parameter that determines tank uplift and corresponding compressive demand in the shell, the shell thickness and material yield strength are also important in determining buckling capacity. In Fig. 3, the relationship between tank geometry and likelihood for buckling failure is highlighted as the Vernier and Rumlang tanks result in the highest susceptibility for shell buckling. The Vernier tank has the highest slenderness ratio (H/R = 3.48) and thinnest shell of all the tank geometries considered, and the Rumlang tank, while less slender than the Birsfelden tank, contains a large volume of liquid (the largest of all four tanks) that when combined with the 16mm shell thickness results in an increased susceptibility for shell buckling. For a PGA of 0.4g both the Vernier and Rumlang tanks have nearly 100% probability of experiencing a shell buckling failure.

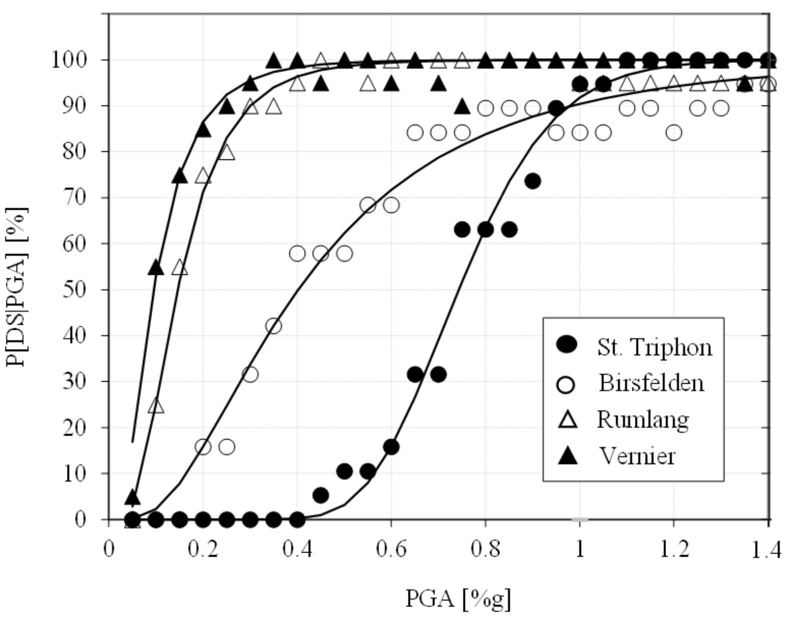

Fig. 3 – Shell buckling fragility curves for all four tanks.

8. Conclusions

A simplified mass-spring model was introduced for the dynamic analysis of unanchored liquid storage tanks, and used to develop fragility curves for probabilistic damage estimation. The introduced model simulates resistance to uplift, tank rocking, and provides an equilibrium-based approach for determining tank shell compressive forces. Four existing tanks were analyzed under 20 recorded ground motions, scaled at 30 different levels (from 0.05g to 1.5g), for a total of 2,400 dynamic analyses. The fragility curves, generated by incremental dynamic analysis of the four tanks, revealed that increased tank slenderness and or larger liquid storage volumes increase the probability of having shell local buckling failure during moderate seismic events. The Vernier and Rumlang tanks, having H/R ratios of 3.78 and 1.75 respectively, suggest shell instability at PGAs of 0.3g and higher. The Vernier tank had the lowest volume (2,080m^3) and highest slenderness, while the Rumlang tank had the highest volume (18,600m^3) and near lowest slenderness.

9. References

[1] Jacobsen, L. S. (1949): Impulsive hydrodynamics of fluid inside a cylindrical tank and of fluid surrounding a cylindrical pier. *Bulletin of the Seismological Society of America*. **39** (3), 189-203.

[2] Housner, G. W. (1963): The dynamic behavior of water tanks. *Bulletin of the Seismological Society of America*. **53** (2): 381-387.

[3] NZSEE (2009): Seismic Design of Storage Tanks. *New Zealand National Society for Earthquake Engineering*. Wellington, New Zealand.

[4] EC8-4 (1998b): Eurocode 8 Part 4: Silos, Tanks, and Pipelines. ENV 1998-4. *European Committee for Standardization*. Brussels, Belgium.

[5] Fujikazu, S., Akira, I., Hajime, H., and Yukio, M. (1988): Experimental study on uplifting behavior of flat-based liquid storage tanks without anchors. *Proc. 9th World Conference on Earthquake Engineering*. Tokyo-Kyoto, Japan**.** 649-654.

[6] Clough, R. N., and Niwa, A. (1979): Static tilt tests of tall cylindrical liquid storage tanks. *EERC 79/06: Earthquake Engineering Research Centre (EERC).*

[7] Clough, D. P., Clough, R.W. (1978): Earthquake Simulator Studies of Cylindrical Tanks. *Nuclear Engineering and Design*. **46** (2): 367-380.

[8] Baker, J.W. (2015): Efficient analytical fragility function fitting using dynamic structural analysis. *Earthquake Spectra* **31**(1):579–599

[9] EC8-1 (1998a): Eurocode 8 Part 1: General rules, seismic actions and rules for buildings. ENV 1998-1. *European Committee for Standardization*. Brussels, Belgium.